

Article

Human Impacts on Holocene Vegetation and Wetland Degradation in the Lower Pearl River, Southern China

Yaze Zhang ¹, Yanwei Zheng ^{1,*}, Qinghua Gong ¹, Shuqing Fu ¹, Cong Chen ², Yongjie Tang ² , Xiao Zhang ², Qiuchi Wan ², Kangyou Huang ²  and Zhuo Zheng ^{2,*} 

¹ Guangdong Open Laboratory of Geospatial Information Technology and Application, Guangzhou Institute of Geography, Guangdong Academy of Sciences, Guangzhou 510070, China

² School of Earth Sciences and Engineering, Sun Yat-sen University, Zhuhai 519082, China

* Correspondence: zhengyanwei@gdas.gd.cn (Y.Z.); eeszzhuo@mail.sysu.edu.cn (Z.Z.)

Abstract: Reconstructing Holocene vegetation history and human impact on vegetation is critical for understanding past interactions between humans and nature. This study concentrates on the lower West River area in Southern China, offering high-resolution reconstructions of vegetation changes over the last 9000 years. Our findings reveal that during the Holocene Climatic Optimum (9–5 ka BP), the area was predominantly covered by dense evergreen broad-leaved forests. Around 5.1 ka BP, the emergence of marsh forests, as evidenced by abundant pollen of *Glyptostrobus* and *in situ* buried woods and roots, indicated a transition towards a wetland ecosystem. Notably, a thriving wetland environment and high production of peat deposits dating from 4.3 ka to 2.5 ka BP reflect the continuous drop of lake levels and the formation of swamps driven by a climatic pattern marked by decreased precipitation, potentially linked to a reduction in summer monsoon intensity during the latter part of the Holocene. This period of wetland expansion also coincides with the earliest evidence of rice cultivation in Southern China, suggesting a relationship between agricultural development and regional landscape changes. Additionally, millennial-scale paleo-megafloods are not only identified by lithological features but also by pollen taxa and principal component analysis. Despite the temporary disruptions of the marsh forest, it demonstrated resilience, quickly recovering within decades. By approximately 2.5 ka BP, a significant increase in rice-type Poaceae pollen and Pteridophyte spores, alongside the sharp decline of *Glyptostrobus* and a decrease in arboreal taxa, were observed. This shift in pollen spectra, coupled with a PC1 curve of principal component analysis, points to intensified human activity as a primary driver behind the collapse of the local wetland ecosystem. These findings align with regional evidence from the Pearl River Delta and coastal Southern China, highlighting extensive human intervention in natural forests and the onset of large-scale agriculture post-2.5 ka BP.

Keywords: Holocene; Pearl River; pollen record; vegetation reconstruction; wetland ecosystem; human impact



Citation: Zhang, Y.; Zheng, Y.; Gong, Q.; Fu, S.; Chen, C.; Tang, Y.; Zhang, X.; Wan, Q.; Huang, K.; Zheng, Z. Human Impacts on Holocene Vegetation and Wetland Degradation in the Lower Pearl River, Southern China. *Land* **2024**, *13*, 530. <https://doi.org/10.3390/land13040530>

Academic Editor: Mark Altaweel

Received: 6 March 2024

Revised: 12 April 2024

Accepted: 12 April 2024

Published: 16 April 2024



Copyright: © 2024 by the authors. Licensee MDPI, Basel, Switzerland. This article is an open access article distributed under the terms and conditions of the Creative Commons Attribution (CC BY) license (<https://creativecommons.org/licenses/by/4.0/>).

1. Introduction

The West River (WR), the longest mainstream of the tributaries within the Pearl River system, flows downstream into the South China Sea via the Pearl River Delta (PRD). It is situated in the southern subtropical zone, and the region's vegetation dynamics are markedly sensitive to the intensity of summer monsoons and the hydrological cycle. The interplay between land cover, Holocene climatic fluctuations, and human activities raises several concerns of increasing academic interest.

The East Asian Monsoon (EAM), one of the most dynamic climatic systems in the study region, exhibits patterns closely aligned with summer insolation trends, peaking during the early Holocene before diminishing [1–4]. Contrasting evidence, particularly from pollen data, indicates that the Holocene Thermal Maximum (HTM) spanned approximately 8–4 ka BP [5]. Some research suggests the possibility of a time-transgressive

Holocene optimum across Eastern China [5–7]. However, the primary patterns of Holocene vegetation changes remain elusive, especially in the lowland areas at the southern boundary of the subtropical zone. New pollen data from the lower reaches of the Pearl River could elucidate detailed vegetation responses to Holocene monsoonal climate variations, thereby distinguishing the effects of human impact on forest transitions.

As early as the 1980s, Huang et al. [8,9] conducted a primary investigation of Holocene buried fossil wood distribution sites in the PRD, followed by more systematic and comprehensive research by Li et al. [10]. Over the past few decades, large quantities of peat, buried wood, roots, and other plant residues have been discovered from the sediments in the Pearl River Delta due to excavations for corks, flower fertilizer, river sand extraction, fish ponds, and other construction projects. The identified fossil wood (*Glyptostrobus pensilis*) represents a swamp forest in a fluvial back-marsh environment during the mid-to-late Holocene. The Holocene peaty deposits containing wood fossils are predominantly found in lowland areas at the landward head of the PRD, particularly within its West and North River tributaries [11], which have drawn considerable scientific attention.

Recently, based on *in situ* buried stumps and pollen assemblages from the Xinxing River drainage area (a tributary of the lower West River), the Holocene marsh forest community dominated by *Glyptostrobus pensilis* has been reconstructed [12]. However, given that *G. pensilis* in modern natural populations is now an endangered species, there is an ongoing debate regarding their historical migration process during the late Holocene [11].

Post-glacial climate changes have profoundly influenced regional vegetation [5], yet the transition from the mid-to-late Holocene saw agricultural development becoming increasingly dominant in driving land cover changes, particularly in lowland regions [13,14]. The timing of early rice cultivation in China remains contentious. The domesticated-type spikelet bases found at Kuahuqiao archaeological site have already shown that rice cultivation had begun by 8000 ka BP, followed by the subsequent spread of rice cultures [15–17]. Some new studies and archaeological excavations suggest that the inception of rice agriculture predates > 10 ka BP in the Yangtze River's lower reaches [18]. The subsequent southward migration of rice farmers significantly contributed to the genetic and linguistic diversity of Southeast Asia [19]. Nevertheless, the role of early rice cultivation in ecosystem changes within the Pearl River regions, south of the Yangtze, remains ambiguous despite AMS ¹⁴C dating of carbonized seed remains from key South China archaeological sites indicating the introduction of domesticated rice around 5000 years ago [20]. The debate continues over whether climate fluctuations or human activities were the primary drivers of vegetation changes in Southern China during the mid-to-late Holocene. Thus, elucidating the contributions of climatic dynamics and anthropogenic factors to regional vegetation shifts is imperative.

This paper investigates a Holocene peaty deposit profile within a river terrace nestled among the hilly terrain of a minor tributary in the lower West River, Southern China. Through detailed pollen analysis, we aim to reconstruct the historical vegetative landscape, local marsh forests, and early agricultural development. Our study addresses critical scientific queries: What were the patterns of zonal forest succession and the principal trends in summer monsoon rainfall during the Holocene at the interface of tropical and subtropical zones? How did the marsh forests and wetland ecosystem expand and contract? Furthermore, what was the linkage between wetland degradation and Neolithic human activities, as well as the processes of human impacts on local vegetation?

2. Geographic Settings

The Pearl River basin stands as one of the most significant river systems in Southern China. The delta's flatlands are intricately woven with a network of tributaries and distributaries, pivotal to the PRD, which encompasses three primary tributaries: the West, North, and East Rivers (Figure 1A). The confluence of the North and West Rivers in Sanshui feeds into the Pearl River, whereas the East River directly merges into the Pearl River. The WR within the Pearl River basin, originating deep within the Yunnan mountainous plateau

in the west and flowing downstream into the South China Sea via the PRD, extends over 2214 km and encompasses a drainage region of 353,100 km². Notably, the WR contributes to approximately 77.8% of the total drainage area of the Pearl River system [21]. As far west as Zhaoqing from the upper delta, exhibiting broad river basin features due to the narrow channel of Lingyang Gorge (Figure 1C), the WR showcases the diverse geomorphology and rich ecological tapestry of the region.

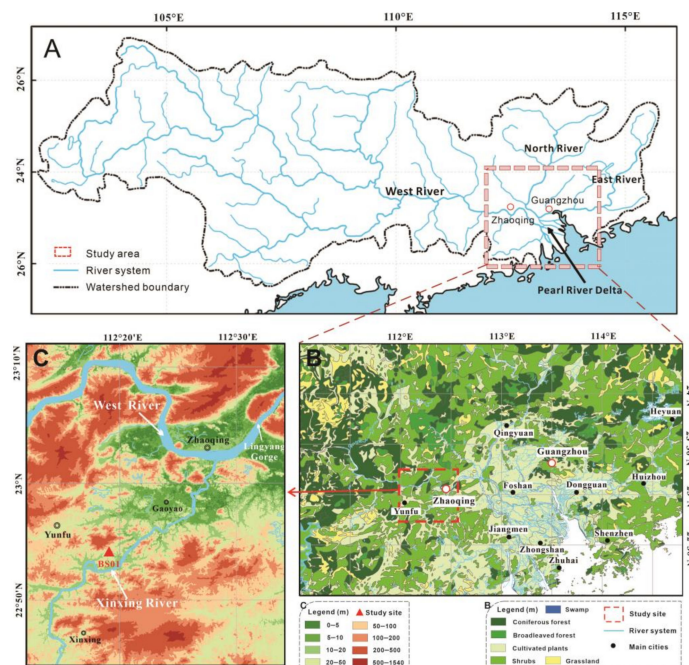


Figure 1. Topography and vegetation maps of the study area. (A) Area of the Pearl River catchment system showing the West, North and East Rivers, the Pearl River Delta and the study area. (B) Regional vegetation map and location of the study area. (C) Topography map showing the lower reaches of the West River and Xinxing tributary watercourse.

A tributary of the lower WR, the Xinxing River extends approximately 145 km and converges with the WR near the Zhaoqing Basin (Figure 1C). This drainage area near Gaoyao is notable for its hilly topography and thick Holocene peat deposits, nestled in lowland depressions between hills and mountains on either side of the Xinxing River terrace. Rich in plant fragments and woods of *Glyptostrobus*, this area, colloquially termed “the underground forest,” has been extensively excavated for applications such as corks and gardening fertilizer [10].

The regional geomorphological structure of the study area can be broadly categorized into three distinct zones: the southern zone, marked by hills and mountains, with bedrock that is mainly Tertiary red sandstone; the central zone, characterized by expansive floodplains, the so-called Zhaoqing Basin; and the northern zone, delineated by a series of northeast to southwest-oriented folded mountain ranges. Elevations in the surrounding low hills of the study area remain below 150 m, with numerous depressions or small lakes and peat deposits scattered throughout the foothills.

Climatically, the study area lies near the Tropic of Cancer and the southern part of the subtropical zone. The climate is dominated by monsoon circulation with abundant rainfall during the summer. The average annual temperature is approximately 22 °C, and the main rainy season occurs from April to October each year with a mean annual precipitation of 1600–1800 mm [11,22]. Due to the instability of the low-latitude atmosphere, convective weather with thunderstorms frequently occurs in this area. The predominant natural vegetation is tropical and southern subtropical evergreen broad-leaved forests [23]. Due to human activities, many areas are affected and covered by secondary forests, secondary shrubs, and artificial vegetation like *Pinus elliottii*. Common plant species include tropical plant species

from families such as Palmae, Myrtaceae, Moraceae, Lauraceae, and Melastomataceae. Typical subtropical evergreen broad-leaved trees observed in the protected vegetation reserve of Dinghu include families from Fagaceae (esp. *Castanopsis*, *Lithocarpus*, and *Cyclobalanopsis*), Lauraceae (*Cryptocarya*, *Machilus*, *Michelia*, and *Phoebe*), Theaceae (*Schima* and *Eurya*), Euphorbiaceae (*Mallotus*, *Macaranga*, *Aporosa*, and *Alchornea*), Myrtaceae (*Syzygium*), Ulmaceae (*Gironniera*), Araliaceae (*Schefflera*), Sapotaceae (*Sarcosperma*), Melastomataceae (*Blastus*), Rubiaceae (*Psychotria* and *Aidia*), Proteaceae (*Helicia*), Hamamelidaceae, and many other taxa [24]. The lowlands, now predominantly covered by intensively planted forests and agricultural cultivation, are mainly distributed with *Pinus massoniana*, *Cinnamomum cassia*, *Illicium verum*, *Dimocarpus logan*, *Arachis hypogaea*, *Saccharum sinense*, and rice [23].

3. Material and Methods

The study area is located between the primary river flat basin of Zhaoqing in the WR and the depressions amidst the hilly terrain along the lower Xinxing River. Core BS01, positioned near Baizhu Town, southwest of Gaoyao City (22.890° N, 112.330° E, 14.02 m above sea level), lies approximately 300 m from the Xinxing River's watercourse. An 820 cm long peat-deposit profile was meticulously extracted from a section within the excavation pit located in the lowland depression. Samples of the continuous deposit were carefully collected and secured in halved PVC tubes (15 cm × 50 cm).

In this region, radiocarbon dating through accelerator mass spectrometry (AMS ¹⁴C) on various materials sourced from local peat deposits indicated that fine organic matter and micro-charcoals yield more reliable dating results compared to wood fragments or fine roots [12,25]. Consequently, ¹⁴C samples were analyzed by Beta Analytic, Ltd., and bulk organic matter was selected for analysis to establish the chronology of core BS01. To eliminate *in situ* root residues and large plant fragments that might have penetrated multiple sediment layers, the bulk samples were sieved through a 180 μm mesh prior to undergoing the standard acid–base–acid (ABA) pretreatment for AMS ¹⁴C dating. Radiocarbon ages were calibrated using CALIB 8.2 software [26], defining “cal. a BP” as calibrated years before the present (i.e., 1950 AD) for this study. Given the rapid deposition observed in flood deposit layers and the relatively stable sedimentation rate of peat, a linear interpolation method was employed to construct the age model.

Core BS01 samples were collected at 2 cm intervals, then dried and placed in a 2 cm × 2 cm × 2 cm cubic polyethylene box for the measurement of bulk density and mass magnetic susceptibility (MS). Bulk density was calculated by dividing weight by volume, whereas MS was assessed using a Bartington MS2 susceptibility meter. Low-frequency MS (0.465 kHz) was measured in volume-specific SI units and normalized for sample mass, with each sample's MS measurements repeated thrice to ensure reproducibility and reliability.

For palynological analysis, samples were extracted at 4–6 cm intervals. Pollen and spores were isolated by employing a standard palynological processing technique, which included heavy liquid separation [27]. To ascertain palynology concentrations, a tablet of *Lycopodium* spores (batch no. 27637) was added to each sample [28]. Samples, each weighing 1 g dry, were sieved through a 125 μm mesh to eliminate fine and coarse particles, treated with 10% HCl to remove carbonates, 48% HF at room temperature to dissolve silicates, and 10% KOH in an 80 °C water bath to degrade organic matter. The remaining sediment was further processed through heavy liquid separation to isolate pollen and spores, which were then preserved in plastic tubes with glycerin jelly. Each sample's general terrestrial pollen count exceeded 400 grains, with percentages of each pollen and spore taxon calculated separately against the total terrestrial pollen sum. Pollen of Poaceae with grain sizes > 35 μm were identified as river-type Poaceae, indicative of rice cultivation. Fossil pollen grains of Taxodiaceae were morphologically compared with those of the contemporary wetland plant *Glyptostrobus pensilis* using scanning electron microscopy (SEM), confirming their consistency. The stratigraphically unconstrained incremental sum of squares cluster analysis (CONISS) was applied to delineate the pollen assemblage zones, with the analytical process and pollen diagrams executed in TILIA 2019 software [29].

Principal Components Analysis (PCA) was utilized to distill the pollen and spore data into a two-dimensional plot, showcasing the taxa distribution. This study's PCA analysis aimed to elucidate the palynological composition in relation to ecosystem development and delineate the interplay between vegetation dynamics and human influence [30]. Pollen and spore taxa that reached abundances of over 5% at least once were included in the analysis. The outcomes of the statistical analyses were visualized using CANOCO 5 software [31].

4. Results

4.1. Lithology and Chronology

The core length for BS01 extends to approximately 8 m beneath the cultivated ground surface, and the stratigraphy reveals three primary sedimentary units upward (Figure 2).

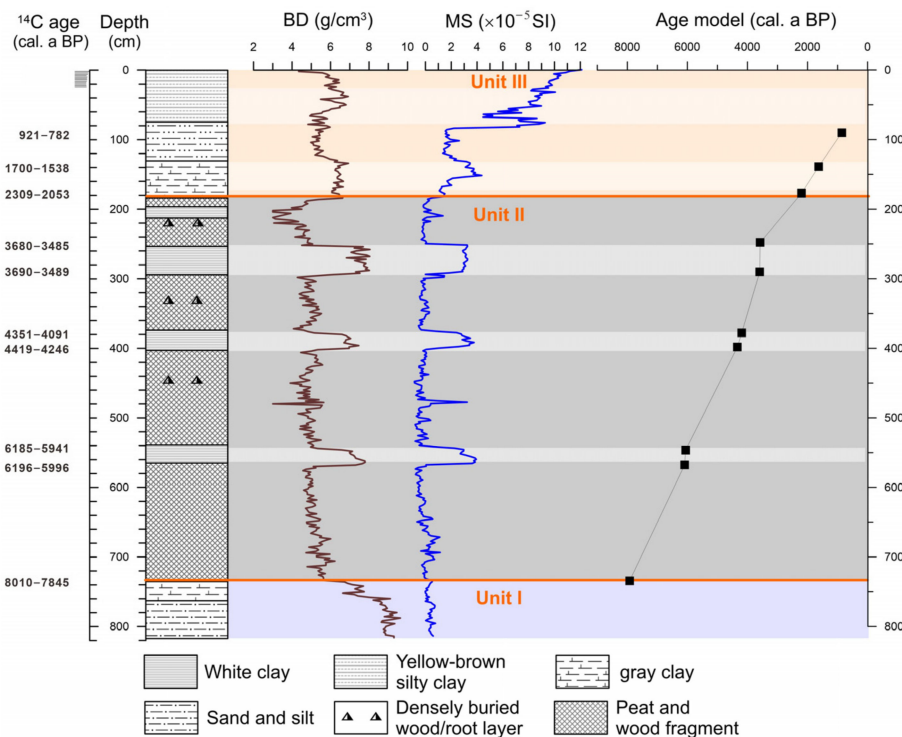


Figure 2. Lithology, sediment bulk density (BD), magnetic susceptibility (MS), and age–depth model of the profile BS01.

Unit I (820–736 cm depth), located near the base of the profile, consists of high-density sandy silt. There is more sand in the bottom, with increasing gray clay on the top of this unit. The lowest part of the sediment profile (820–750 cm) has a higher bulk density (BD) but relatively low magnetic susceptibility (MS). The sediment is primarily composed of high-density sandy silt, with BD values reaching up to 7–9 g/cm³ but showing a decreasing trend upward. The MS value exhibits relatively minor fluctuations in this unit.

Unit II (736–184 cm) comprises a thick peat deposit containing abundant plant fragments and *in situ* buried trunk bases and roots of *Glyptostrobus*. The peat deposits are generally of low bulk density. A series of layers of pure, white-to-light-gray clay are interbedded in this dark peat sediment unit. The bulk density and the magnetic susceptibility of these white clay layers are much higher than those of the peaty sediment. The BD value contrast is most prominent in this unit where peat deposits have the lowest bulk density, averaging 4–5 g/cm³, while the BD in clay layers has values as high as 7–8 g/cm³. The peaty sediment shows very low MS values, averaging a slight oscillation between –0.5 and 0.5 SI. However, it shows significantly high values in the clay layers, reaching as high as 2.5–4 SI.

Unit III (182–0 cm), the uppermost unit transitioning to the plowed surface soil, is characterized by gray silty clay. There is more silt and clay on the bottom, increasing sand the component in the middle, and yellow-brown silty clay on the top. The bulk density is relatively

higher than in Unit II, probably because of less organic matter content. There is a relative increase with a narrowing values gap in two different deposits, averaging 4.5–5.5 g/cm³ in the peaty sediments and 6–7 g/cm³ in the clays, respectively. There is a substantial increase in MS values. In the top-most gray-white clay layer, the MS value fluctuates between 5 and 8 SI, subsequently increasing towards the top of the core to reach 12 SI (Figure 2).

Most importantly, the intercalated layers of white-to-light-gray clay in the peaty sediment of BS01 are 5 to 40 cm thick. The bulk density and magnetic susceptibility exhibit noticeable stratigraphic variations between clay sediment and peat deposits, with significantly higher values in the former, indicating differences in sediment sources. The peat deposit is generally organic-rich and may have lower magnetic susceptibility compared to more mineral-rich sediments like white-to-light-gray clay in BS01. Chen et al. [12] conducted a multi-proxy analysis of profiles in the nearby area around the Xinxing River and found that the total organic carbon (TOC) content and pollen concentration in the white-to-light-gray clay layers were both very low, almost devoid of organic matter, which is markedly different from the organic-rich peat deposits. The sediment particles in the clay layers are fine, well-sorted, and exhibit low skewness. The dominant clay minerals are kaolinite, illite, and chlorite. Such mineral composition is similar to that found in sediments of nearby rivers, floodplains, or river terraces in the Xinxing River and in the lower WR near the Zhaoqing Basin.

A total of 10 AMS ¹⁴C dates were obtained from the BS01 core (Table 1). Samples for ¹⁴C AMS dating were selected from several intervals with distinct lithological changes, as well as from the top and bottom of gray-white clay layers. The dating results from the top and bottom of different clay layers (BS01–6 and 7, BS01–8 and 9, BS01–10 and 11) with a thickness of 20–40 cm differing by only a few decades, which suggests that each gray-white clay layer represents a sudden event. This age difference was due to the upper contact of the clay layer was the organic-rich peat deposit. The chronological framework adopts linear interpolation based on 10 dating results.

Table 1. Radiocarbon dates from profiles BS01 (modified from [12]).

Depth (cm)	Sample	Lab. No	Age (ka BP)	±2σ (cal. ka BP)	Median (cal. ka BP)	Median (BC/AD)
90	BS01-3	BETA369885	940 ± 30	921–782	851	1099 AD
139	BS01-4	BETA389737	1720 ± 30	1700–1538	1606	344 AD
177	BS01-5	BETA389738	2170 ± 30	2309–2053	2179	229 BC
248	BS01-6	BETA369886	3350 ± 30	3686–3485	3547	1624 BC
290	BS01-7	BETA369887	3360 ± 30	3689–3489	3592	1642 BC
378	BS01-8	BETA389739	3810 ± 30	4351–4091	4198	2248 BC
398	BS01-9	BETA389740	3910 ± 30	4419–4246	4346	2396 BC
546.5	BS01-10	BETA369888	5280 ± 30	6185–5941	6079	4129 BC
567.5	BS01-11	BETA369889	5310 ± 30	6196–5996	6085	4135 BC
734.5	BS01-12	BETA369890	7100 ± 40	8010–7845	7932	5982 BC

4.2. Result of Pollen Analysis

Palynological results reveal distinct shifts in pollen assemblages, highlighting a clear succession of vegetation over the past 9000 years (Figure 3). The study samples, generally rich in pollen, identified 108 taxa with concentrations exceeding 100,000 grains/g in the peat sediments. The assemblages were overwhelmingly dominated by arboreal taxa, such as *Cyclobalanopsis*, *Castanopsis*, *Glyptostrobus*, Euphorbiaceae, and non-arboreal taxa of Cyperaceae and Poaceae. Fern spores typically exhibited a higher proportion relative to pollen in the clay layers, with the most common taxa of *Dicranopieris*, *Cibotium*, and *Polypodium*. Based on the preferred habitats of the pollen- and spore-producing plants, we categorized them into tropical trees (TR), subtropical trees (ST), temperate trees (TP), wetland species (WT), gymnosperms (GYM), herbs (HB), and pteridophytes (PT). The stratigraphically unconstrained incremental sum of squares cluster analysis (CONISS) delineated five zones (I–V) and two subzones based on the percentage of pollen and spore taxa (Table 2 and Figure 3).

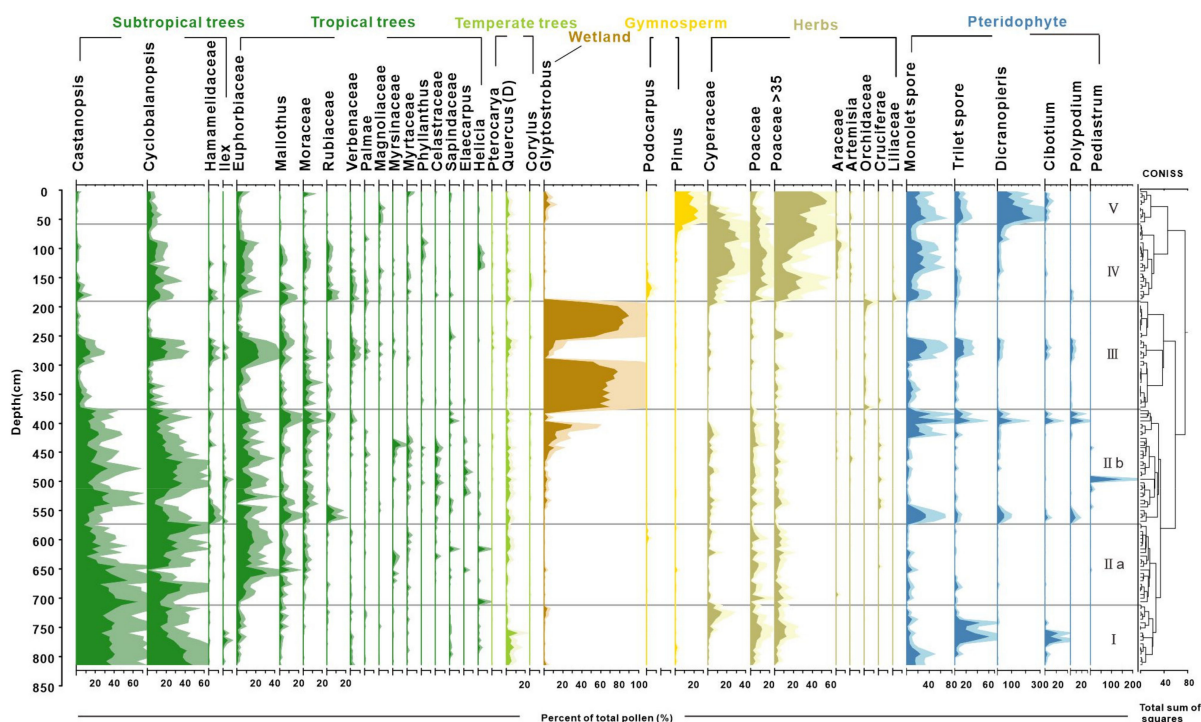


Figure 3. Detailed pollen diagram of principal pollen taxa from BS01.

Zone I (820 to 718 cm, cal. 9.0 to 7.8 ka BP) was dominated by the taxa indicative of a dense subtropical broad-leaved evergreen forest (*Castanopsis*, *Cyclobalanopsis*, and *Quercus*). The tropical tree pollen is present only in trace amounts. *Poaceae* (~24%) pollen was prevalent within the herb group. Notably, *Cyperaceae* contributions increased up to 14.5% in the upper part of this zone.

Zone II (718 to 384 cm, cal. 7.8 to 4.3 ka BP) exhibited a continuous high abundance of *Cyclobalanopsis* and *Castanopsis* pollen, alongside an increase in tropical tree pollen. Tropical taxa were primarily composed of *Euphorbiaceae*, *Mallothus*, and *Moraceae*, with a slight decline in *Euphorbiaceae* observed in subzone IIb compared to IIa. *Glyptostrobos* pollen, indicative of wetland environments, surged to approximately 30% in the upper part of subzone IIb before experiencing a sudden decline in the clay layer. Fern spores significantly increased only at the top and bottom samples of white clay sediments, with *Pediastrum* peaking at a depth of 496 cm.

Zone III (384 to 192 cm, cal. 4.3 to 2.5 ka BP) was marked by significant increases in *Glyptostrobos* pollen of hygrophilous trees, with a peak at 216 cm (90%). In a thick clay bed within the zone, *Glyptostrobos* drastically reduced to an average of 7%, associated with the substitution of fern spores and other terrestrial pollen taxa.

Zone IV (from 192 to 60 cm, cal. 2.5 to 0.6 ka BP) is characterized by sedge-dominated wetland and herb pollen, mostly contributed by *Poaceae* (up to 55%) and *Cyperaceae* (up to 29%), and an increase in monolete spores. It is important to note that there was a primary increase of rice-type *Poaceae* pollen (>35 μ m) to >10% in the lower part and >30% in the upper part (since cal. 900 cal. BP) of this zone. Subtropical and tropical trees reappeared, with the main contributions being from *Cyclobalanopsis* and *Euphorbiaceae*.

Zone V (from 60 to 2 cm, before 0.6 ka BP) shows a fluctuating increase in rice-type *Poaceae* pollen, reaching up to 55% in the top samples. Wetland pollen *Cyperaceae* decreases notably during this interval, whereas gymnosperm pollen *Pinus* (averaging 18%) and fern spore *Dicranopteris* become the main contributors in this interval and increase up to their highest abundances.

In summary, the pollen record chronicles a gradual transformation from a dense broad-leaved evergreen forest during the Holocene climate optimum to a local swampy *Glyptostrobos* forest, culminating in an open environment dominated by grassy wetlands.

The disappearance of swamp and wetland environments over the last millennia was likely due to soil erosion induced by early farming development on the lower river terrace. Additionally, the significant proportions of rice-type Poaceae starting around 900 cal. ka BP suggest a local transition from sedge and grassland cover to rice paddy fields.

Table 2. List of main taxa identified in core BS01.

Tropical Trees	Subtropical Trees	Wetland
Apocynaceae	<i>Altingia</i> [Altingiaceae]	Alismataceae
Bignoniaceae	Anacardiaceae	<i>Glyptostrobus</i> [Cupressaceae]
Caesalpiniaceae	<i>Aralia</i> [Araliaceae]	Iridaceae
Celastraceae	Caprifoliaceae	Lobeliaceae
Dipterocarpaceae	<i>Castanopsis</i> [Fagaceae]	<i>Nuphar</i> [Nymphaeaceae]
<i>Elaeocarpus</i> [Elaeocarpaceae]	<i>Cyclobalanopsis</i> [Fagaceae]	Onagraceae
<i>Phyllanthus</i> [Euphorbiaceae]	Combretaceae	<i>Polygonum</i> [Polygonaceae]
<i>Mallotus</i> [Euphorbiaceae]	Crypteroniaceae	<i>Typha</i> [Typhaceae]
Euphorbiaceae	Elaeagnaceae	
Flacourtiaceae	Hamamelidaceae	Herbs
Guttiferae	<i>Ilex</i> [Aquifoliaceae]	Araceae
<i>Helicia</i> [Proteaceae]	<i>Myrica</i> [Myricaceae]	<i>Artemisia</i> [Asteraceae]
Loranthaceae	<i>Rhamnus</i> [Rhamnaceae]	Chenopodiaceae
Lythraceae	Rosaceae	Commelinaceae
Magnoliaceae	Scrophulariaceae	Convolvulaceae
Melatomataceae	Theaceae	Cruciferae
<i>Melia</i> [Meliaceae]	Thymelaeaceae	<i>Impatiens</i> [Balsaminaceae]
Mimosaceae	<i>Ulmus</i> [Ulmaceae]	Lamiaceae
Moraceae		Liliaceae
Myrsinaceae	Temperate Trees	Orchidaceae
Myrtaceae	<i>Alnus</i> [Betulaceae]	Poaceae
<i>Nyssa</i> [Nyssaceae]	<i>Betula</i> [Betulaceae]	Ranunculaceae
Oleaceae	<i>Corylus</i> [Betulaceae]	Saururaceae
Palmae	<i>Pterocarya</i> [Juglandaceae]	Cyperaceae
Papilionaceae	<i>Quercus</i> (D) [Fagaceae]	
Passifloraceae	Ulmaceae	Pteridophyte
<i>Reevesia</i> [Sterculiaceae]		<i>Cibotium</i> [Cibotiaceae]
Rubiaceae		<i>Dicranopteris</i> [Gleicheniaceae]
Rutaceae	Gymnosperm	<i>Diplazium</i> [Gleicheniaceae]
Sapindaceae	<i>Podocarpus</i> [Podocarpaceae]	<i>Lycopodium</i> [Lycopodiaceae]
Sapotaceae	<i>Pinus</i> [Pinaceae]	<i>Lygodium</i> [Lygodiaceae]
<i>Symplocos</i> [Symplocaceae]		<i>Polypodium</i> [Polypodiaceae]
Tiliaceae		<i>Pediastrum</i> [Pediastraceae]
Verbenaceae		Concentricytes

4.3. Principal Component Analysis of Pollen Data

PCA was performed on the relative frequencies of pollen to discern the primary factors influencing vegetation dynamics. Analysis of 34 taxa across 136 samples from the BS01 record yielded the first four principal components (PCs) with relatively modest eigenvalues, collectively accounting for 41.35% of the variance. The eigenvalues for these components are 14.23%, 10.95%, 9.27%, and 6.9%, respectively. Relatively small eigenvalues for the first two components underscore the complexity of the factors impacting pollen assemblages at the study site, encompassing climatic changes, sedimentary events (paleo-megafloods), and anthropogenic influences. Taxa exhibiting negative loadings on PC1 predominantly include common pollen taxa from tropical and subtropical evergreen broad-leaved forests, such as *Castanopsis*, *Ilex*, Myrsinaceae, *Mallotus*, *Cyclobalanopsis*, Moraceae, Hamamelidaceae, and Euphorbiaceae. Conversely, taxa with positive loadings on PC1 are characteristic of crops and

open vegetation, including Poaceae, Cyperaceae, *Pinus*, *Artemisia*, and Araceae. This pattern suggests that PC1 largely reflects the interplay between moisture conditions and human intervention in vegetation dynamics.

According to the PCA result, the *Glyptostrobus* variable exhibits the highest negative values in PC2 and PC4, making it the most influential taxon across multiple PCA axis loads. Notably, *Glyptostrobus* from peat sediments plays a crucial role in pollen assemblages throughout the record. The key distinction lies in the fact that taxa at the opposite end of *Glyptostrobus* primarily consist of taxa from shrubs and lowland vegetation in PC2, while Pteridophyte spores dominate PC4. Figure 4 illustrates that taxa with positive loadings for PC2 include Rubiaceae, Hamamelidaceae, Verbenaceae, *Mallothus*, Palmae, and Euphorbiaceae, indicating trees and shrubs under humid conditions. These components reflect both local pollen sources (*in situ* growth marsh forest and adjacent evergreen forest) versus regional lowland vegetation (Figure 4a,b). In contrast, for PC4, major taxa with positive loadings mainly comprise Pteridophytes and plants from regional evergreen forests such as *Castanopsis*, *Quercus*, *Cyclobalanopsis*, Sapindaceae, *Pinus*, etc., suggesting a contrasting relationship between local marshes of the *Glyptostrobus* forest with fern spores (mostly transported by floods) and forest pollen taxa with broader distribution ranges. Taxa exhibiting positive loadings for PC3 encompass lowland and marsh forest plants like *Glyptostrobus*, Orchidaceae, Verbenaceae, *Mallothus*, and Pteridophyte; whereas those displaying negative loadings are predominantly composed of evergreen broad-leaved forest plants, including *Cyclobalanopsis*, Celastraceae, Myrtaceae, and *Castanopsis* (Figure 4c,d). The significance of PC3 may lie in representing a transition from broad-leaved forests to wetland forests at a local scale.

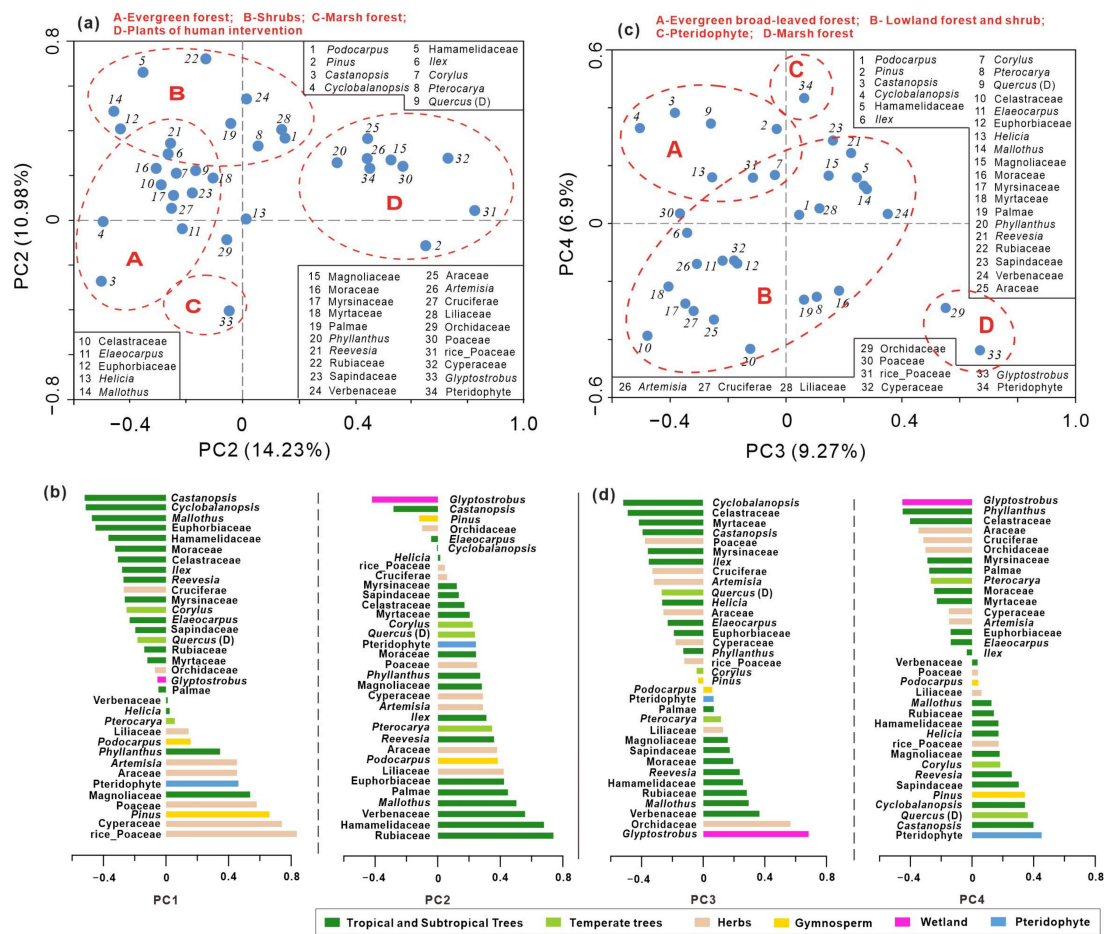


Figure 4. Principal component analysis (PCA) ordination based on percentage values of 34 pollen taxa. (a) Scatter plot of the first two axes (PC1 vs. PC2); (b) PC1 and PC2 scores of the selected pollen taxa; (c) scatter plot of the axis PC3 and axis PC4; (d) PC3 and PC4 scores of the selected pollen taxa.

5. Discussion

5.1. Holocene Predominance of Evergreen Broad-Leaved Forest and the Development of a Marsh Forest

Since ~9 ka BP, the pollen analysis indicates a predominance of arboreal taxa from evergreen broad-leaved forests. The relatively low concentration of pollen, the abundant presence of fern spores, and the sandy/silty sediment phase suggest the initial stages of a small lake influenced by surface flow and streams from nearby hilly land areas. From around 7.8–4.3 ka BP (pollen zone II), the vegetation type inferred for the study area still consisted mainly of dense evergreen broad-leaved forests but exhibited an abundance of tropical arboreal elements such as Euphorbiaceae, *Mallothus*, and Moraceae (Figures 3 and 5). This may reflect a warm and humid climate condition during the middle Holocene in this region. Such climatic conditions are broadly synchronous with the well-known Holocene Thermal Maximum (HTM) [32], characterized by enhanced summer monsoons in the Northern Hemisphere and high melting rates of polar ice sheets [33]. During the early stages of HTM, marine transgression reached its maximum extent along coastal regions. Deltaic sedimentary and microfossil data suggest that around 8–7 ka BP marked the highest stand of Holocene marine transgression, while mountains and hills directly bordered the paleo-estuary coastline at the mouth of the Pearl River [14]. A number of studies propose that the upper delta areas had already experienced inundation by Holocene transgression along incised valleys as early as approximately 9 ka BP [11,34,35].

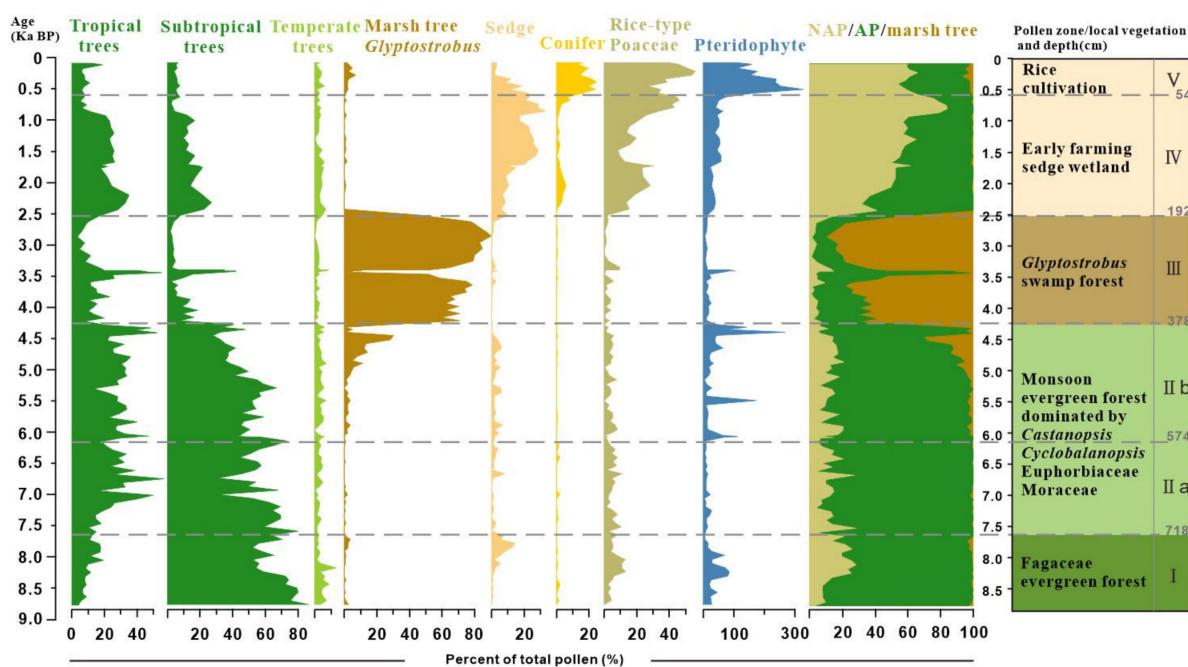


Figure 5. Pollen group and synthetic diagram of the profile BS01.

From approximately 4.3 to 2.5 ka BP, the local small basin underwent a transformation from an evergreen broad-leaved forest into a marsh coniferous forest, as evidenced by the abundant presence of *Glyptostrobus* pollen constituting 60–80% of the total pollen in zone III (Figures 3 and 5). Additionally, a large amount of buried woods and *in situ* *Glyptostrobus* stumps and roots were found in peaty deposits. The development of the initial marsh forest occurred around 5.1 ka BP, with its subsequent dominance since approximately 4.3 ka BP coinciding with the declining trend of summer insolation during the Holocene of the Northern Hemisphere (Figure 6). A similar pattern of high *Glyptostrobus* pollen abundance was also observed in another nearby pollen record [22]. The external factors contributing to wetland forest development are likely complex [36–38]. Firstly, speleothem $\delta^{18}\text{O}$ data from Chinese caves indicate a gradual weakening of Asian summer monsoon intensity over the past 6000 years [1–3], suggesting reduced annual rainfall leading to shallower lake water

levels. Secondly, sediment filling may have caused water overflow in our study area since approximately 5.1 ka BP. The above climatic and sedimentary factors collectively contributed to extensive marsh development and widespread distribution of *Glyptostrobus* forests. Such a vegetation process indicated by our pollen record aligns well with the formation and expansion patterns of the wetland system observed around the Pearl River Delta.

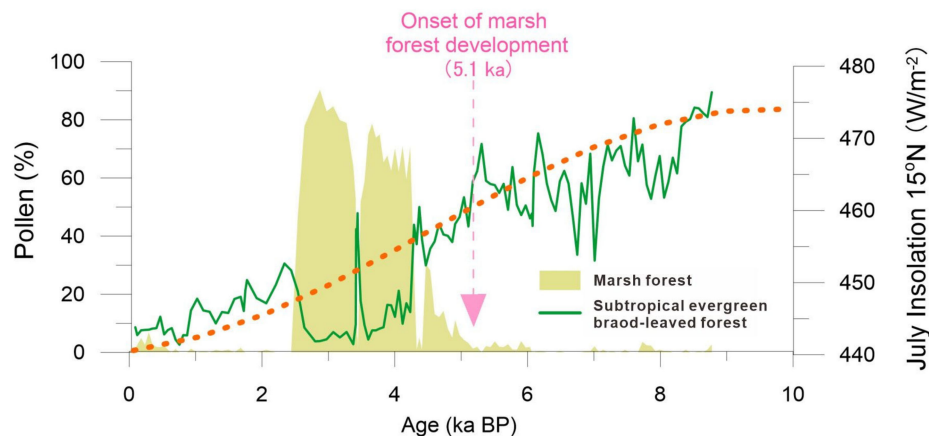


Figure 6. The pollen decline trend of an evergreen broad-leaved forest during the Holocene compared with July insolation, showing that the rapid flourishing of the marsh forest since cal. 5.1 ka BP may be related to the weakening of the summer monsoons.

A previous study demonstrated increasing sediment discharge from the West River and North River during the mid-to-late Holocene period, particularly after cal. 5–4 ka BP [31]. Since the reduction in available space for sedimentary accommodation, the deltaic floodplain initiated its formation. The increased flow at the river outlet was primarily influenced by river runoff, and the relatively high water table in the delta facilitated the rapid development of freshwater marshes and lakes in the upper deltaic region. Consequently, due to fluvial aggradation, the lake became shallower and transformed into a large, waterlogged depression suitable for hygrophilous plant growth. Extensive freshwater swamps formed in downstream areas of the West and North Rivers during the mid-to-late Holocene after the maximum marine transgression. From a contemporary perspective on ecology and distribution, the marsh plant of *Glyptostrobus* tends to thrive abundantly along riverbank lakes and stream bend wetlands, with hydrodynamics serving as its primary environmental condition of propagation [39]. During this period, marsh forests dispersed along freshwater systems to expand their distribution range within the upper delta areas. Numerous buried woods of *Glyptostrobus* have been discovered across interconnected regions, exhibiting paleo-environmental control [8,11]. Other than *G. pensilis*, other trees such as *Cinnamomum camphora*, *Bischofia javanica*, *Castanopsis* spp., and *Cyclobalanopsis* spp. were also identified among these buried woods [39]. In our study area, pollen from *Glyptostrobus* primarily occurred around cal. 5.1 ka BP, with a significant increase over the subsequent millennia (4.3–2.5 ka BP) coinciding with its occurrence in the upper delta areas of the North Pearl River [11].

5.2. History of Human Activity and Degradation of Marsh Forest Ecosystem

A significant and important change in pollen spectra demonstrates that the flourishing *Glyptostrobus* marsh forest since about 5.1 ka BP was followed by a sharp degradation at cal. 2.5 ka BP, which coincides with rapid rice farming development in the region (Figure 7) and the acceleration of delta plain growth in the mouth of the Pearl River [35,40,41]. According to the AMS ^{14}C dating results of carbonized rice remains at Neolithic archaeological sites in Southern China, rice farming had spread southward by ~5 ka BP, followed by continued expansion into coastal areas of the South China Sea. The Neolithic evidence of rice cultivation in the Shixia and Chaling archaeological sites has been dated to 5.0–4.7 ka BP [42], which are also the earliest rice remains in the upstream areas of the Pearl River Delta. This early introduction of rice cultivation in Southern China is broadly synchronous with the

large wetland development, mostly covered by *Glyptostrobus* marsh forest. However, the natural monsoonal evergreen forest was not significantly damaged by early farming during this period, and the marsh forest was approximately undisturbed during 5–2.5 ka BP. This implies that the disturbance of human activities to the natural vegetation and surrounding landscape was still weak when agriculture had not yet become the main economic form during the late Neolithic period, which has been demonstrated by many archaeological artifact features [43]. A previous synthetic study shows that the extensive expansion of rice farming in coastal Southern China significantly lagged behind that of the lower Yangtze River [14]. Although rice remains have been found at numerous archaeological excavations during the period from 5000 to 4000 cal. ka BP (Figure 7a), the unearthed artifacts are generally associated predominantly with fishing and gathering economies [43–45].

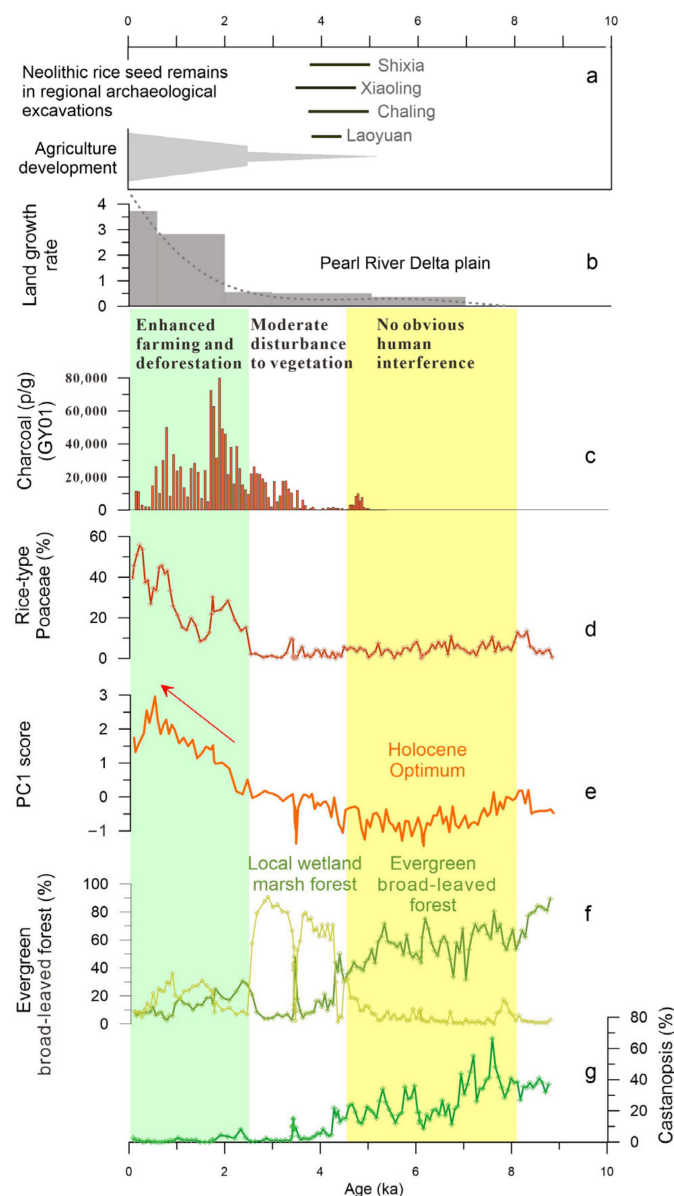


Figure 7. Human impact on local vegetation and its comparison with early rice evidence and delta plain growth during the Holocene. (a) ^{14}C age ranges of carbonized rice seeds in regional Neolithic sites; (b) land growth rate of the Pearl River Delta [35]; (c) charcoal concentration from the record GY01 [22]; (d) rice-type pollen percentage value; (e) PC1 score as human activity index; (f) pollen group proportions of evergreen broad-leaved forest and marsh forest plus wetland sedge; (g) *Castanopsis* content, a key pollen taxon of evergreen broad-leaved plant.

The top-most pollen assemblage reflects a significant human impact on vegetation. The marsh forest, which had developed for nearly 3000 years from about 5.1 ka BP, decreased sharply at about 2.5 ka BP and almost disappeared from the local area at about 2.1 ka BP. Obviously, such a collapse of the *Glyptostrobus* forest wetland ecosystem can be related to the development of rice farming. The PC1, as an index of human activity, together with the rice-type Poaceae, also began to rise from 2.5 ka BP, clearly indicating the progressive strengthening of human impact on local vegetation. Charcoal concentrations recorded in the near profile GY01 indicate an increase in fire frequency starting around 3.5 ka BP [18], reaching a peak around 2.1–1.8 ka BP, indicating that the prehistoric inhabitants surrounding the PRD likely initiated extensive slash-and-burn cultivation during the past two thousand years. Intensive fire occurrences have been closely linked to human activities [46] and must be the primary factors leading to the destruction of natural vegetation. The growth of natural *Glyptostrobus* forests is very dependent on or sensitive to changes in local water levels. This mode of growth and distribution also makes them vulnerable to destruction in unusual landscape changes (such as soil erosion) caused by agricultural development. It was suggested that since the Qin and Han Dynasties, a large number of northern immigrants brought agricultural technology, associated with the rapid growth of the delta plain that led to an increase in land available for farming [14,35,47]. Since freshwater wetland provides good soil and land for rice cultivation, the *Glyptostrobus* forest has been extensively destroyed and converted into paddy fields. This, together with the expansion of arable land plains and population growth, has been the main mechanism triggering land cover changes for the past few thousand years.

5.3. Pollen Data as an Indicator of Megaflood Deposition

A correlation based on multiple sediment proxies and stratigraphic analyses between at least three sites (including BS01) revealed that there were at least seven megaflood events in the lower West River in the past 6000 years (Figure 8). These well-dated megafloods correspond to once-in-a-thousand-year events with an average return period of approximately 855 years [12]. In this current paper, we additionally show the detail and statistical features of pollen assemblages in the megaflood layers. In the study profile BS01, many “once-in-a-millennium” flood events are recorded by interbedded white clay layers. During the paleo-megaflood inundations, the *in situ* marsh forest was submerged and damaged, whereas, according to the high-resolution AMS ^{14}C ages and pollen result, the wetland ecosystem recovered rapidly after each flooding disaster within a few decades.

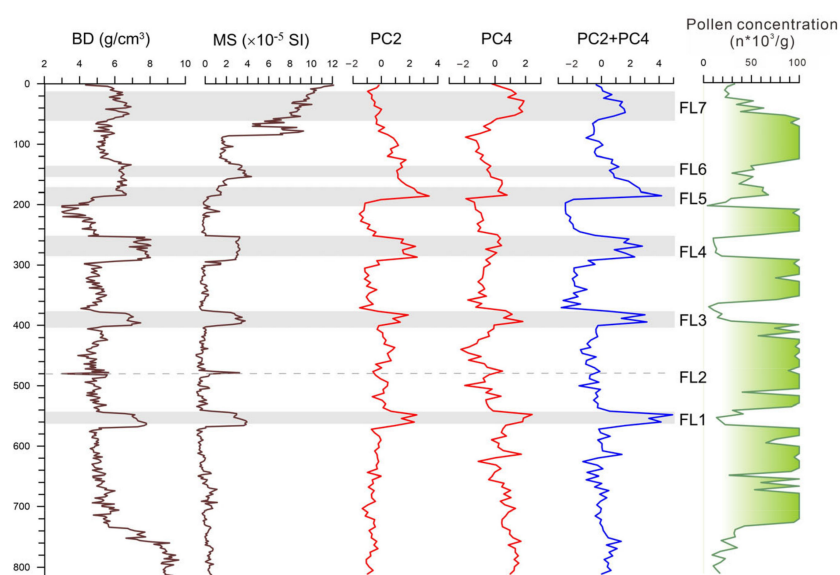


Figure 8. Indicative significance of principal component analysis of pollen taxa to megaflood layers (FL1–FL7).

Pollen analysis in this study also found that pollen assemblage is a good marker of flood events. Pollen records in the white clay deposits are characterized by an increase in fern spores and regional vegetation taxa of relatively long-distance transportation, which is distinctly different from the local swamp forest dominated by *Glyptostrobus* (Figure 5). Such abrupt pollen percentage changes from the taxa of local swamps to those of longer-distance origins show that the clay beds contain more pollen grains transported from a larger source range during the flooding period.

It was suggested that each gray-white clay layer interbedded with black wood-rich peat layers was characterized by very fine sediment derived from suspended loads of a megaflood. Exceptionally high water levels during flood periods caused the overflow of the Xinxing River and the inundation of valleys on both sides. Such exceptional megafloods transported a substantial amount of suspended fine sediment carried by the river flow to rapidly deposit in the study area's hilly terrace valley, forming distinct gray-white clay layers that differ significantly from local wetland peat deposits.

To better understand the relationship between pollen assemblage and paleo-megaflood deposits in the study site, we compared the PC2 and PC4 curves to bulk density (BD) and mass magnetic susceptibility (MS). The results show that the curves in the PCA are closely related to pollen concentration (significantly fewer pollen grains in the flood sediment layers), which can be correctly mirrored in those of the BD and MS data. Among the principal components, the PC2 and PC4 scores in the flood layers are exceptionally high compared to those of the peat deposits, suggesting that the PC2 and PC4 can be used as good indicators of megaflood events (Figures 4 and 8).

The marsh tree of *Glyptostrobus* is characteristic because it presents the extreme value of negative loading in the above two principal component axes (Figure 4). In the PC2, the taxa with the largest positive load values are those from natural rainforest elements such as Rubiaceae, Hamamelidaceae, Verbenaceae, Palmae, and so on. The PC2 score shows higher values in the flood layers, except FL7, which remained relatively low (Figure 8). Taking into consideration the high proportion of rice-type Poaceae pollen in the FL7 event, which is rare in the other flood layers, the PC2 indicator of flooding may be invalid due to deforestation caused by increased human activities. Meanwhile, in the PC4, Pteridophyte is located in the positive maximum, which may be directly linked to fluvial sedimentation because a majority of spores were transported by water runoff, not by wind, indicating strengthened fluvial transportation and sedimentation [48]. On the whole, most rainforest pollen taxa have high eigenvalues in the positive loading of PC2 and fern spores in PC4 (Figure 4). In contrast, *Glyptostrobus* has the highest eigenvalues in the negative loading of both PC2 and PC4, contributing to the indication that PC2 and PC4 can be regarded as indicators of megaflood events.

6. Conclusions

The high-resolution vegetation reconstruction of the past 9000 years revealed a series of land cover changes around the lower West River caused by climate variation and human activity. During the Holocene climatic optimum (9–5 ka. BP), local vegetation was dominated by evergreen broad-leaved forests with rich tropical elements. A distinct change in pollen assemblages shows that a marsh forest dominated by *Glyptostrobus* began to develop at about 5.1 ka BP and became prevalent in this wetland system between 4.2 ka and 2.5 ka BP. The wetland formation toward the later part of the Holocene period suggests a climate trend of reduced rainfall, possibly driven by the weakening of summer monsoons.

The development of the marsh forest in the study area is consistent with the main growth period of the wetland ecosystem in the overall lower Pearl River basin, which is approximately synchronous with early rice farming during the late Neolithic revealed by ¹⁴C ages of rice seeds from archaeological sites in Southern China. This implies that the regional wetland expansion was beneficial to the land use for agricultural development of rice cultivation, thus triggering the early migration of agricultural populations into Southern China. Around 2.5 ka BP, coupled with the sharp degradation of the marsh forest

of *Glyptostrobus* and a significant decrease in arboreal taxa, there was a notable rise in rice-type Poaceae and heliophilous fern spores. Associating with PC1 loading of pollen taxa based on principal component analysis, it is suggested that enhanced human activity led to the collapse of the *in situ* wetland ecosystem. The regional records from the Pearl River Delta and coastal Southern China show a consistent result that extensive human intervention in natural forests and large-scale agricultural development occurred after 2.5 ka BP.

In the study area, a series of millennial-scale paleo-megafloods have been identified, which reveals that historical large-scale flooding was a major disaster in the lower West River. Despite the inundation during the paleo-megafllood period, the wetland ecosystem can recover quickly within a few decades. Only under the environment of human interference was the marsh forest destroyed and difficult to restore.

Author Contributions: Conceptualization, Y.Z. (Yaze Zhang), Y.Z. (Yanwei Zheng) and Z.Z.; Methodology, Y.Z. (Yaze Zhang) and Z.Z.; Software, Y.Z. (Yaze Zhang) and Z.Z.; Formal analysis, Y.Z. (Yanwei Zheng) and Z.Z.; Investigation, Y.Z. (Yaze Zhang), Y.Z. (Yanwei Zheng), S.F., C.C., Y.T., X.Z., Q.W., K.H. and Z.Z.; Writing—original draft, Y.Z. (Yaze Zhang); Writing—review & editing, Y.Z. (Yaze Zhang), Y.Z. (Yanwei Zheng) and Z.Z.; Funding acquisition, Y.Z. (Yanwei Zheng), Q.G. and Z.Z. All authors have read and agreed to the published version of the manuscript.

Funding: This study was supported by the National Natural Science Foundation of China (NSFC Grants 42072205, 41301582); the National Key R&D Program of China (2022YFF0801501); the Innovation Group Project of Southern Marine Science and Engineering Guangdong Laboratory (Zhuhai) (Grant No. 311020002); and the Science and Technology Development Project of Guangdong Academy of Sciences (2022GDASZH-2022010104).

Data Availability Statement: The original contributions presented in the study are included in the article, further inquiries can be directed to the corresponding authors.

Acknowledgments: Thanks to Ping-Ri Li for his suggestions and advice on research work.

Conflicts of Interest: The authors declare no conflict of interest.

References

1. Dykoski, C.A.; Edwards, R.L.; Cheng, H.; Yuan, D.; Cai, Y.; Zhang, M.; Lin, Y.; Qing, J.; An, Z.; Revenaugh, J. A high-resolution, absolute-dated Holocene and deglacial Asian monsoon record from Dongge Cave, China. *Earth Planet. Sci. Lett.* **2005**, *233*, 71–86. [[CrossRef](#)]
2. Wang, Y.; Cheng, H.; Edwards, R.L.; He, Y.; Kong, X.; An, Z.; Wu, J.; Kelly, M.J.; Dykoski, C.A.; Li, X. The Holocene Asian monsoon: Links to solar changes and North Atlantic climate. *Science* **2005**, *308*, 854–857. [[CrossRef](#)] [[PubMed](#)]
3. Hu, C.; Henderson, G.M.; Huang, J.; Xie, S.; Sun, Y.; Johnson, K.R. Quantification of Holocene Asian monsoon rainfall from spatially separated cave records. *Earth Planet. Sci. Lett.* **2008**, *266*, 221–232. [[CrossRef](#)]
4. Wang, Y.; Cheng, H.; Edwards, R.L.; Kong, X.; Shao, X.; Chen, S.; Wu, J.; Jiang, X.; Wang, X.; An, Z. Millennial- and orbital-scale changes in the East Asian monsoon over the past 224,000 years. *Nature* **2008**, *451*, 1090–1093. [[CrossRef](#)] [[PubMed](#)]
5. Zheng, Z.; Chen, C.; Huang, K.; Zhang, X.; Kershaw, P.; Cheng, J.; Li, J.; Yue, Y.; Wan, Q.; Zhang, Y.; et al. Holocene warming and evergreen/deciduous forest replacement across eastern China. *Quat. Sci. Rev.* **2023**, *307*, 108057. [[CrossRef](#)]
6. An, Z.; Porter, S.C.; Kutzbach, J.E.; Wu, X.; Wang, S.; Liu, X.; Li, X.; Zhou, W. Asynchronous Holocene optimum of the East Asian monsoon. *Quat. Sci. Rev.* **2000**, *19*, 743–762. [[CrossRef](#)]
7. Herzschuh, U.; Winter, K.; Wünnemann, B.; Li, S. A general cooling trend on the central Tibetan Plateau throughout the Holocene recorded by the Lake Zigetang pollen spectra. *Quat. Int.* **2006**, *154–155*, 113–121. [[CrossRef](#)]
8. Huang, Z.; Li, P.; Zhang, Z.; Li, K. Wood-rich peat layers of Quaternary system in Pearl River Delta. *Trop. Geogr.* **1981**, *2*, 50–55. (In Chinese)
9. Huang, Z.; Li, P.; Zhang, Z.; Li, K.; Qiao, P. *Formation, Development and Evolution of the Pearl River Delta*; Popular Science Press, Guangzhou Branch: Guangzhou, China, 1982. (In Chinese)
10. Li, P.; Cui, H.; Tan, H.; Dai, J.; Shen, C.; Sun, Y. A study on Holocene buried timbers in Guangdong. *Trop. Geogr.* **2001**, *21*, 195–197. (In Chinese)
11. Zheng, Z.; Tang, Y.; Zheng, Y.; Huang, K.; Han, Z.; Zong, Y.; Li, P.; Tan, H. Environmental Changes Inferred from Spatial-temporal Distribution of Holocene Buried Peat Layers in Lower Reaches of the Xijiang and Beijiang and the River Confluence of Pearl River Delta. *Trop. Geogr.* **2016**, *36*, 313–325. (In Chinese)
12. Chen, C.; Zheng, Y.; Zheng, Z.; Zong, Y.; Huang, K.; Rolett, B.V.; Peng, H.; Zhang, X.; Tang, Y.; Wan, Q.; et al. Holocene millennial-scale megafllood events point to ENSO-driven extreme climate changes. *Sci. China Earth Sci.* **2023**, *66*, 2530–2545. [[CrossRef](#)]

13. Chen, C.; Zhao, W.; Xia, Y.; Gu, Q.; Yu, W.; Zhang, Y.; Wu, D.; Liu, J.; Zhang, X. History of human disturbance to vegetation in the Southeast Hills of China over the last 2900 years: Evidence from a high resolution pollen record. *Palaeogeogr. Palaeoclimat. Palaeoecol.* **2022**, *598*, 111028.
14. Ma, T.; Rolett, B.V.; Zheng, Z.; Zong, Y. Holocene coastal evolution preceded the expansion of paddy field rice farming. *Proc. Natl. Acad. Sci. USA* **2020**, *117*, 24138–24143. [[CrossRef](#)]
15. Fuller, D.Q.; Harvey, E.; Qin, L. Presumed domestication? Evidence for wild rice cultivation and domestication in the fifth millennium BC of the Lower Yangtze region. *Antiquity* **2007**, *81*, 316–331. [[CrossRef](#)]
16. Fuller, D.; Qin, L.; Zheng, Y.; Zhao, Z.; Chen, X.; Hosoya, L.; Sun, G. The domestication process and domestication rate in rice: Spikelet bases from the Lower Yangtze. *Science* **2009**, *323*, 1607–1610. [[CrossRef](#)] [[PubMed](#)]
17. Fuller, D. Pathways to Asian civilizations: Tracing the origins and spread of rice and rice cultures. *Rice* **2011**, *4*, 78–92. [[CrossRef](#)]
18. Lu, H.Y. New methods and progress in research on the origins and evolution of prehistoric agriculture in China. *Sci. China Earth Sci.* **2017**, *60*, 2141–2159. [[CrossRef](#)]
19. Lipson, M.; Cheronet, O.; Mallick, S.; Rohland, N.; Oxenham, M.; Pietruszewski, M.; Pryce, T.O.; Willis, A.; Matsumura, H.; Buckley, H.; et al. Ancient genomes document multiple waves of migration in Southeast Asian prehistory. *Science* **2018**, *361*, 92–95. [[CrossRef](#)] [[PubMed](#)]
20. Yang, X.; Wang, W.; Zhuang, Y.; Li, Z.; Ma, Z.; Ma, Y.; Cui, Y.; Wei, J.; Fuller, D.Q. New radiocarbon evidence on early rice consumption and farming in South China. *Holocene* **2017**, *27*, 1045–1051. [[CrossRef](#)]
21. Tong, J. The Generalizations and Hydrological Character Analysis of Pearl River Basin. *Water Conserv. Sci. Technol. Econ.* **2007**, *13*, 31–33. (In Chinese)
22. Peng, H.; Zheng, Z.; Zheng, Y.; Huang, K.; Wei, J. Holocene vegetation changes and human activities revealed by a peat sediment core in Gaoyao, Zhaoqing. *Quat. Sci.* **2015**, *35*, 742–754. (In Chinese)
23. Wu, Z.Y. *Vegetation of China*; Science Press: Beijing, China, 1980.
24. Zou, S.; Zhou, G.Y.; Zhang, Q.M.; Meng, Z.; Chu, G.W.; Xu, S.; Xia, Y.J. Long-term (1992–2015) dynamics of interspecific associations among tree species in a monsoon evergreen broad-leaved forest in Dinghushan Biosphere Reserve. *Acta Ecol. Sin.* **2019**, *39*, 6362–6371. (In Chinese) [[CrossRef](#)]
25. Shen, C.; Ding, P.; Wang, N.; Yi, W.; Ding, X.; Fu, D.; Liu, K.; Zhou, L. Buried ancient forest and implications for paleoclimate since the mid-Holocene in South China. *Radiocarbon* **2010**, *52*, 1411–1421. [[CrossRef](#)]
26. Stuiver, M.; Reimer, P.; Reimer, R. CALIB rev. 8.2. Available online: <http://calib.org/> (accessed on 4 April 2022).
27. Nakagawa, T.; Brugiapaglia, E.; Digerfeldt, G.; Reille, M.; Beaulieu, J.; Yasuda, Y. Dense-media separation as a more efficient pollen extraction method for use with organic sediment/deposit samples: Comparison with the conventional method. *Boreas* **1998**, *27*, 15–24. [[CrossRef](#)]
28. Stockmarr, J. Tablets with Spores used in Absolute Pollen Analysis. *Pollen Spores* **1971**, *13*, 615–621.
29. Grimm, E.C. CONISS: A FORTRAN 77 Program for stratigraphically constrained cluster analysis by the method of incremental sum of squares. *Comput. Geosci.* **1987**, *13*, 13–35. [[CrossRef](#)]
30. Birks, H.J.B.; Frey, D.G.; Deevey, E.S. Review 1: Numerical tools in palaeolimnology—Progress, potentialities, and problems. *J. Paleolimnol.* **1998**, *20*, 307–332. [[CrossRef](#)]
31. Ter Braak, C.J.F.; Smilauer, P. *CANOCO Reference Manual and CanoDraw for Windows User's Guide: Software for Canonical Community Ordination (Version 4.5)*; Microcomputer Power: Ithaca, NY, USA, 2002.
32. Zhou, X.; Sun, L.; Zhan, T.; Huang, W.; Zhou, X.; Hao, Q.; Wang, Y.; He, X.; Zhao, C.; Zhang, J.; et al. Time-transgressive onset of the Holocene Optimum in the East Asian monsoon region. *Earth Planet. Sci. Lett.* **2016**, *456*, 39–46. [[CrossRef](#)]
33. Renssen, H.; Seppä, H.; Crosta, X.; Goosse, H.; Roche, D.M. Global characterization of the Holocene Thermal Maximum. *Quat. Sci. Rev.* **2012**, *48*, 7–19. [[CrossRef](#)]
34. Zong, Y.; Huang, G.; Switzer, A.D.; Yu, F.; Yim, W.W.S. An evolutionary model for the Holocene formation of the Pearl River delta, China. *Holocene* **2009**, *19*, 129–142. [[CrossRef](#)]
35. Tang, Y.; Zheng, Z.; Huang, K.; Chen, C.; Chen, Z.; Lu, H.; Wu, W.; Lin, X.; Zhang, X.; Li, H. Holocene Evolution of the Pearl River Delta: Mapping Integral Isobaths and Delta Progradation. *J. Mar. Sci. Eng.* **2023**, *11*, 1986. [[CrossRef](#)]
36. Qu, X.; Huang, C.; Rao, Z.; Wu, L.; Luo, Y.; Chen, F.; Li, Y.; Zhao, L.; Liu, L.; Song, Z.; et al. Natural and anthropogenic controls on environmental change during the Holocene based on a multiproxy record obtained from subalpine peatland in southern China. *Sci. Total Environ.* **2024**, *912*, 169446. [[CrossRef](#)] [[PubMed](#)]
37. Chen, C.; Li, H.; Wei, L.; Ji, Y.; Wu, S.; Xu, Q.; Zhao, W.; Zhang, X.; Zhao, Y. Rate of vegetation change in southeast China during the Holocene and its potential drivers. *Rev. Palaeobot. Palynol.* **2024**, *322*, 105066. [[CrossRef](#)]
38. Xiao, J.; Lu, H.; Zhou, W.; Zhao, Z.; Hao, R. Evolution of vegetation and climate since the last glacial maximum recorded at Dahu peat site, south China. *Sci. China Earth Sci.* **2007**, *50*, 1209–1217. [[CrossRef](#)]
39. Li, P.; Cui, H.; Tan, H.; Feng, Y.; Liu, H.; Mu, Z.; Sun, Y.; Song, L. Climate and Environmental Changes Reflected by Buried Ancient trees in Guangdong. *Geomorphology, Environment and Development*. In *Proceedings of the 2004 Danxia Mountain Conference*; The Geographical Society of China: Nanjing, China, 2004.
40. Zong, Y.; Zheng, Z.; Huang, K.; Sun, Y.; Wang, N.; Tang, M.; Huang, G. Changes in sea level, water salinity and wetland habitat linked to the late agricultural development in the Pearl River delta plain of China. *Quat. Sci. Rev.* **2013**, *70*, 145–157. [[CrossRef](#)]

41. Zheng, Z. Study of human disturbance to the vegetation in recent thousands of years in the coastal areas of southeast China. *Ecol. Sci.* **1998**, *17*, 30–36.
42. Yang, X.; Chen, Q.; Ma, Y.; Li, Z.; Hung, H.; Zhang, Q.; Jin, Z.; Liu, S.; Zhou, Z.; Fu, X. New radiocarbon and archaeobotanical evidence reveal the timing and route of southward dispersal of rice farming in south China. *Sci. Bull.* **2018**, *63*, 1495–1501. [[CrossRef](#)] [[PubMed](#)]
43. Huang, G. Neolithic culture and paleogeographic environment in the Zhujiang Delta. *Acta Geogr. Sinica* **1996**, *51*, 508–517. (In Chinese)
44. Zhao, S. Environmental change and cultural evolution of the Pearl River Delta in Pre-Qin period. *Huaxia Archaeol.* **2007**, *2*, 90–97. (In Chinese)
45. Xia, X.; Zhang, P.; Wu, Y. The analysis of rice remains from the Chaling site in the Pearl River Delta, Guangdong Province. *Quat. Sci.* **2019**, *39*, 24–36. (In Chinese)
46. Guo, X.; Zhao, W.; Sun, J.; Li, F.; Zhang, K.; Zhao, Y. Advances of Charcoal Study for Paleoenvironment in China. *J. Glaciol. Geocryol.* **2011**, *33*, 342–348.
47. Xiong, H.; Zong, Y.; Huang, G.; Fu, S. Human drivers accelerated the advance of Pearl River deltaic shoreline in the past 7500 years. *Quat. Sci. Rev.* **2020**, *246*, 106545. [[CrossRef](#)]
48. Zheng, Z.; Li, Q. Vegetation, climate, and sea level in the past 55,000 years, Hanjiang Delta, Southeastern China. *Quat. Res.* **2000**, *53*, 330–340. [[CrossRef](#)]

Disclaimer/Publisher’s Note: The statements, opinions and data contained in all publications are solely those of the individual author(s) and contributor(s) and not of MDPI and/or the editor(s). MDPI and/or the editor(s) disclaim responsibility for any injury to people or property resulting from any ideas, methods, instructions or products referred to in the content.